Optics Letters

# 150 km fast BOTDA based on the optical chirp chain probe wave and Brillouin loss scheme

YONGKANG DONG,[1,*] BENZHANG WANG,[1] CHAO PANG,[1] DENGWANG ZHOU,[1] DEXIN BA,[1] HONGYING ZHANG,[2,4] AND XIAOYI BAO[3]

[1]National Key Laboratory of Science and Technology on Tunable Laser, Harbin Institute of Technology, Harbin 150001, China
[2]School of Science, Harbin University of Science and Technology, Harbin 150080, China
[3]Fiber Optics Group, Department of Physics, University of Ottawa, Ottawa, Ontario K1N 6N5, Canada
[4]e-mail: zhy_hit@163.com
*Corresponding author: aldendong@gmail.com

Received 6 July 2018; revised 27 August 2018; accepted 27 August 2018; posted 28 August 2018 (Doc. ID 338071); published 21 September 2018

**Distributed long-range Brillouin optical time domain analysis (BOTDA) is an extremely time-consuming sensing scheme, which requires frequency mapping of the Brillouin spectrum and a large number of average times. Here, we propose a fast long-range BOTDA based on the optical chirp chain (OCC) probe wave and Brillouin loss scheme. The OCC-modulated probe wave is enabled by cascading fast-frequency-changing microwave chirp segments head-to-tail, which covers a large frequency range around the anti-Stokes frequency relative to the pump wave. The combination of the OCC technique and Brillouin loss scheme provides several advantages, i.e., fast measurement, a high Brillouin threshold, no additional amplification scheme, and freedom from the nonlocal effect. In the experiment, 6 m spatial resolution, 3.2 s measurement time, and 3 MHz measurement precision were achieved over a 150 km single-mode fiber.** 

***OCIS codes:*** (060.2370) Fiber optics sensors; (060.4370) Nonlinear optics, fibers; (290.5900) Scattering, stimulated Brillouin; (280.4788) Optical sensing and sensors.

https://doi.org/10.1364/OL.43.004679

Brillouin optical fiber sensors have the capacity to resolve more than one million points [1], obtain a high-speed strain sampling rate [2], and achieve a long sensing distance [3]. In applications, long-range distributed Brillouin optical fiber sensors are promising tools to monitor large-scale structures such as power cables, railways, and oil and gas pipelines. BOTDA sensors feature high signal-to-noise ratios (SNRs), which will finally determine the sensing distance. It is obvious that increasing the pump and probe input power improves the SNR. However, nonlinearities in the fiber are the main obstacles to inject high pump and probe power. The pump pulse power should be chosen appropriately in order to avoid modulation instability [4] and self-phase modulation [5], while probe power is restricted by the Brillouin threshold, which drops off with the sensing distance [6]. In addition, the nonlocal effect is another detrimental effect on the long-range performance of the sensors. It is caused by the accumulated interaction between the pump pulse and probe wave, which distorts the Brillouin spectrum and subsequently introduces fitting errors [7]. To extend the sensing range of BOTDA sensors, several impressive technologies have been proposed [8–16]. A well-known technique is to locate the optical repeaters constituted by the erbium-doped fiber amplifiers (EDFA) at critical positions over the sensing distance [8]. The EDFA can also be placed in front of the detector to preamplify the Brillouin signal before detection [9]. Distributed Raman [10] and Brillouin amplifications [11] are other powerful schemes enabling the compensation of fiber loss. Moreover, optical pulse coding [12] and image signal processing [3,13] are effective methods to increase the SNR and extend the sensing distance to the order of 100 km. To achieve long-range Brillouin sensing, the nonlocal effect should be mitigated. The nonlocal effect is introduced during the frequency-scanning process in the Brillouin gain or loss scheme. The power transfer between the pump and probe is high near the fiber Brillouin frequency shift (BFS), while it is low away from the fiber BFS, and this may cause a fluctuation on the pump pulse power that can distort the Brillouin spectrum, especially in the far end of the sensing fiber. Time-division [14] and frequency-division [8] BOTDA systems are able to reduce the Brillouin interaction length, and consequently mitigate the nonlocal effect. In 2016, a BOTDA scheme based on a frequency-modulated probe wave was demonstrated to be free from the Brillouin threshold limitation and detrimental nonlocal effect, which achieved the 100 km sensing distance with 1 megahertz (MHz) measurement accuracy [15]. In the same vein, the frequency–comb modulated probe wave in the Brillouin loss scheme also provides a flat gain, enabling the suppression of the pulse distortion and nonlocal effect [16]. For long-range applications, the response time is also a key property to detect the event and then take remedial actions. However, current long-range BOTDA sensors require frequency mapping of the Brillouin spectrum and a large number of average times, which is a time-consuming process. Besides, some of the existing

0146-9592/18/194679-04 Journal 

long-range BOTDA techniques are forced to sacrifice the measurement time to strengthen the performance in the sensing distance [8,12,14].

Lately, we have introduced a novel single-shot BOTDA sensor based on the OCC technique, which is able to realize distributed strain measurement with a sampling rate up to MHz [17]. The OCC is enabled by cascading the fast-frequency-changing microwave short-chirp segments head-to-tail. The frequency-sweeping span of the microwave short-chirp segment covers several hundred MHz in a few tens of nanoseconds, which can be regarded as the time compression of the frequency-agile microwave signal in the dynamic BOTDA system. The Brillouin gain profile of each fiber segment is received and demodulated by one pump pulse interacting with the corresponding optical chirp segment.

In this Letter, we propose a fast long-range BOTDA sensor based on an OCC probe wave and Brillouin loss scheme, which offers several advantages to achieve good long-range performance. First, the Brillouin spectra can be recovered along the short optical chirp segments in the time domain, so the measurement time is only limited by the pulse repetition rate and average times. Second, the OCC-modulated probe wave owns a wide spectrum, which allows us to increase the SNR by injecting a probe wave power beyond the fiber Brillouin threshold. Next, it is able to compensate the attenuation of the whole pump pulse spectrum along the fiber in the Brillouin loss configuration with no additional amplification scheme. Last, it also overcomes the detrimental nonlocal effect in long-range Brillouin fiber sensing, due to the flat gain of the OCC probe wave. In the experiment, we performed a fast long-range BOTDA sensor capable of a 150 km sensing range, 3.2 s measurement time, and 3 MHz measurement accuracy.

Figure 1 highlights the operation principle of the proposed fast long-range BOTDA sensor based on the OCC technique and Brillouin loss scheme. The OCC modulation is working in the sawtooth mode, where the two adjacent optical short-chirp segments are cascaded by head-to-tail cohesion. Similar to the typical BOTDA system, the pump wave is pulse modulated, and its width is narrower than the duration of the short optical chirp segment ($t_{\text{chirp}}$). The counterpropagating OCC probe wave is injected into the fiber under test (FUT) in the opposite direction. The center frequency difference between the probe wave and pump wave is set near the fiber BFS, and the chirp sweeping frequency span ($f_{\text{chirp}}$) is wide enough to cover the whole Brillouin spectrum. It offers the pump pulse a wide and flat gain along the whole sensing fiber, and the pump power fluctuation in one segment can be ignored. So the proposed technique is free from the nonlocal effect in long-range Brillouin sensing by avoiding the pump pulse distortion and power fluctuation compared with the traditional frequency-scanning process. In each OCC segment, the probe energy is transferred to the pump pulse through Brillouin interaction, so there will be a Brillouin loss spectrum in the time domain. When one fiber segment is heated, the detected signal of that fiber Brillouin loss spectrum peak will move from $t_1$ to $t_2$. The BFS difference $\Delta\nu_{\text{BFS}}$ is given by the time difference,

$$\Delta\nu_{\text{BFS}} = (t_2 - t_1) \times \frac{f_{\text{chirp}}}{t_{\text{chirp}}}. \tag{1}$$

The spatial resolution of the OCC-BOTDA sensor is another important parameter, which is limited by not only the pulse time but also one optical chirp segment time $t_{\text{chirp}}$. Here, the $t_{\text{chirp}}$ dominates the system spatial resolution. Therefore, we should choose the pulse width (40 ns) properly to make sure that the time convolution of the pump pulse and the Brillouin intrinsic spectrum occupied time (8 ns) are less than the $t_{\text{chirp}}$ (60 ns), so the spatial resolution $z_{SR}$ of the OCC-modulated BOTDA scheme is

$$z_{SR} = \frac{c \cdot t_{\text{chirp}}}{2n}. \tag{2}$$

Figure 2 introduces the experimental setup, which employed the dual-modulation method [18] to reduce the arbitrary waveform generator (AWG) bandwidth requirement. The light source was an ultranarrow linewidth-distributed feedback optical fiber laser, operating at a wavelength of 1550 nm. The continuous wave (CW) light was divided by a 90:10 coupler into two branches. In the upper branch, the pump pulse with single-frequency modulation was injected into the FUT from one end. First, the 90% CW light was double-sideband-modulated by an electro-optic-modulator (EOM1), which was driven by a microwave generator (MG) with a frequency of 8.335 GHz. Then the modulated light was intensity modulated by EOM2 to form a 40 ns optical pulse, where the EOM2 was driven by the channel 1 (CH1) of the AWG. Both EOM1 and EOM2 were biased at the minimum transmission working point. Next, the lower sideband of the optical pulse was selected by a tunable fiber Bragg grating (TFBG) working as the pump pulse, and its peak power was amplified to 20 dBm by EDFA1. Finally, the pump pulse was injected into the 150 km fiber through an optical circulator.

In the lower branch with 10% light, the OCC-modulated probe wave was generated and injected into the FUT from the other end. The microwave chirp chain signal was provided by

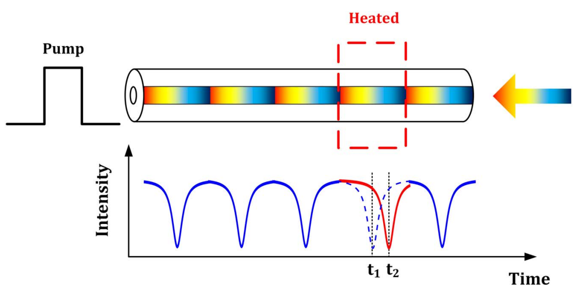


**Fig. 1.** Operation principle of proposed fast long-range BOTDA sensing based on the OCC technique and Brillouin loss scheme.

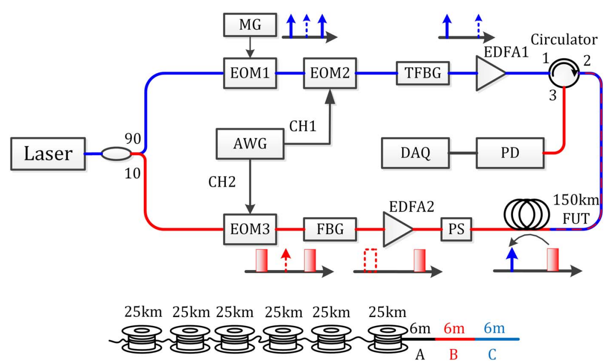


**Fig. 2.** Experimental setup and arrangement of the fiber under test.

channel 2 (CH2) of the AWG, and the chirp span was from 2.4 to 2.695 GHz with a frequency step of 5 MHz. The duration of one optical chirp segment was 60 ns, corresponding to 6 m spatial resolution. CH1 and CH2 of the AWG were synchronized to output the modulating signal, and there was a fixed time delay between them. The EOM3 was also biased at its minimum transmission for double-sideband modulation with the carrier suppressed. The upper sideband of the modulated signal was selected by the narrowband FBG forming the OCC probe wave, and its power was amplified by EDFA2, and then the polarization state was randomized by the polarization scrambler (PS). A probe wave of 10 dBm was launched into the FUT from the other end, whose power was much higher than the Brillouin threshold (about 4 dBm) of the single-frequency probe wave. It was effective to improve the detected SNR with a high probe power and Brillouin amplification through the Brillouin loss scheme, so there was no additional amplification device in the experimental setup.

The 150 km sensing fiber contained six parts, where each one was a 25-km-long single-mode fiber. In the far end, a 6 m fiber segment in position B (shown in Fig. 2) was heated in the oven, while the rest were placed at ambient temperature. Finally, the OCC probe wave was received by a high-gain photodetector with a bandwidth of 75 MHz and collected by data acquisition (DAQ) with a sampling rate of 5 GSa/s. One measurement time was about 3.2 s, while the pulse repetition rate was 625 Hz and the average times were 2000.

The Brillouin trace is obtained in the time domain, and then it can be converted to frequency and length information in the optical chirp segment period. After signal processing, the fiber 3D Brillouin loss spectra over the whole 150 km sensing fiber, which are similar to traditional 3D Brillouin gain spectra, are exhibited as a function of frequency and length shown in Fig. 3(a). Figure 3(b) displays the details of the measured Brillouin loss spectra in three typical positions of 1, 75, and 150 km. It can be seen that the Brillouin signal is observed clearly along the fiber, and the SNR is improved obviously in the last tens of km due to the distributed Brillouin amplification in Brillouin loss configuration. The power is transferred from the OCC-modulated probe wave to the pump pulse, so that the pump pulse is amplified along the fiber, and this can improve the SNR especially in the far end, as shown in the Fig. 3(a). Figure 3(c) displays the zoom-in of the last 100 m fiber Brillouin spectra to show the detail of the Brillouin spectrum in the oven. As a result, it is easy to find the heated fiber at the far end. Noteworthy, the time delay between the pump pulse and the OCC-modulated probe is controlled carefully to guarantee the pump interacts with only one full probe segment in the heated fiber position. Figure 3(d) displays the fiber Brillouin loss spectra in three successive positions (A, B, and C, as shown in Fig. 2), while the spectrum in the dotted red line corresponds to the fiber segment in the oven. We can see that the Brillouin loss spectra before and after the oven overlap very well, while the heated fiber Brillouin loss spectrum is moving right. Moreover, ghost peaks can also be found in Fig. 3, as observed in our previous work, due to the transient SBS interaction [17]. It introduces an oscillation in the acoustic wave, which appears in the high frequency part and fades away in the early part of the next chirp segment. So it distorts the both ends of the Brillouin spectrum pattern. We use the main peak of the Brillouin loss spectrum to extract the BFS, which is able to reduce the fitting error. Next, the fiber Brillouin temperature coefficient should be obtained before we utilize the proposed OCC-BOTDA for quantitative fiber temperature sensing.

The test fiber segment is placed in the oven, and then the temperature is changed from 10°C to 60°C with a temperature step of 10°C. The measured Brillouin loss spectra in every temperature are shown in the inset figure of Fig. 4. It only displays part of the Brillouin loss spectrum about 60 MHz around the main peak, which is used for BFS fitting. The quadratic least squares fitting is employed to give the BFS of each measured Brillouin spectrum. Figure 4 provides the linear fitting result of the fiber BFS variation in different temperatures. The square points in Fig. 4 are the data of the Brillouin loss spectra fitting results subtracting the reference BFS in room temperature. Employing the linear fitting to analyze the relationship between the fiber BFS variation and temperature difference, the fiber temperature coefficient is acquired about 1.06 MHz/°C, which agrees well with the temperature coefficient measured by traditional BOTDA.

Figure 5 depicts the temperature and BFS difference of the last 1 km FUT. It contains three continuous measurement

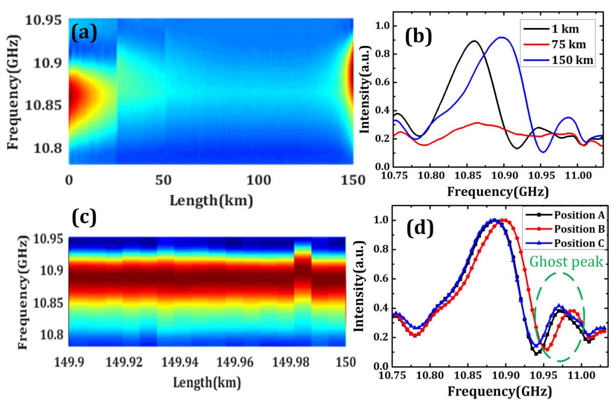


**Fig. 3.** Measured Brillouin loss spectra utilizing the OCC technique and Brillouin loss scheme. (a) The top view of the measured 3D Brillouin loss spectra over the whole 150 km sensing fiber. (b) The Brillouin loss spectra in the position of 1, 75, and 150 km. (c) A zoom-in of the last 100 m fiber of (a) to show the detail of the 3D Brillouin loss spectra in the oven. (d) The measured Brillouin loss spectra in position A, B, and C.

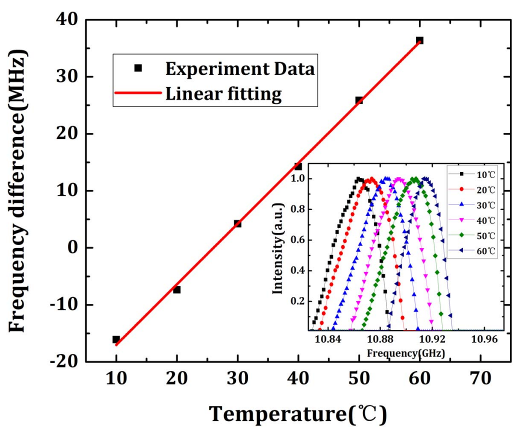


**Fig. 4.** Fiber BFS variation in different temperatures and the linear fitting result.

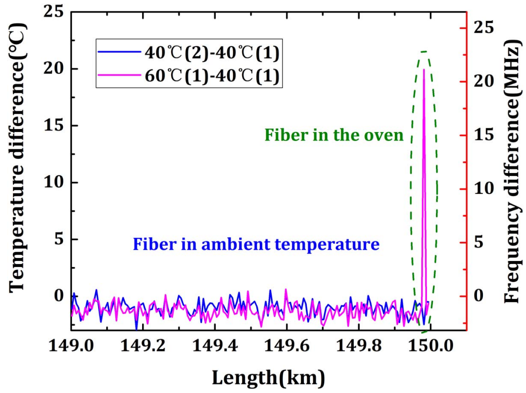


**Fig. 5.** Temperature and BFS difference along the last 1 km sensing fiber in three continuous measurement results.

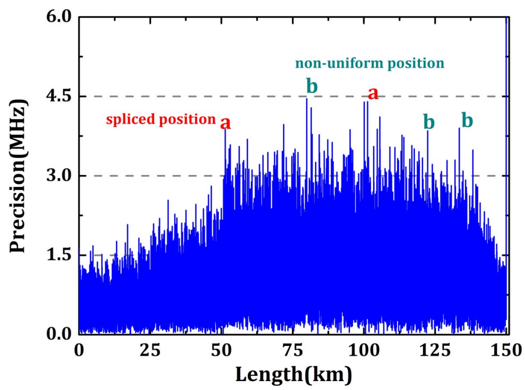


**Fig. 6.** Precision of measured BFS along the 150 km fiber.

results at two different temperatures, while one measurement is set as a reference data. First, the temperature in the oven is set at 40°C, and then two continuous measurements are made. The BFSs of the heated fiber are 10.895 and 10.893 GHz with a measurement uncertainty of 2 MHz. The two measurement results have a good repeatability at the same temperature as the subtracted result is given by the blue curve. Then the temperature of the oven is increased to 60°C. The BFS of the heated fiber becomes 10.916 GHz. The BFS change is about 21 MHz for 20°C temperature vibration. It agrees well with the fiber temperature coefficient 1.06 MHz/°C. The temperature difference is also provided by the same reference and drawn in the pink curve. Here we need to state that the reference data can be obtained before the sensing, so the conclusion of measurement time as 3.2 s can be drawn.

Figure 6 shows the precision of the measured BFS along the 150 km fiber, given by standard deviation of the three continuous measurement results. The measurement precision is high at both ends, while it is poor in the middle. It can be explained that the measurement precision is a function of the Brillouin signal intensity, through Fig. 3(a). The measurement precision is improved at the far end due to the pump pulse amplified by the OCC-modulated probe wave in Brillouin loss configuration. Moreover, the spatial resolution is not high enough to avoid the fitting error at the spliced fiber positions (51 and 100 km) or some nonuniform positions (80, 122, and 133 km) with two different BFS. In Fig. 6, the typical fitting error at spliced positions is marked as "a," while that at the nonuniform positions is marked as "b." As a result, we can draw a conclusion that the measurement precision of the proposed fast long-range OCC-BOTDA is about 3 MHz.

In conclusion, we have demonstrated a fast long-range BOTDA sensor by using the OCC technique and Brillouin loss scheme. The OCC-modulated probe wave with a broadband spectrum has been proved capable of increasing the Brillouin threshold, avoiding the nonlocal effect, and amplifying the pump pulse. A sensing range of 150 km has been realized without any other amplification scheme, obtaining a spatial resolution of 6 m, 3 MHz measurement precision, and 3.2 s measurement time with 2000 averaging. The AWG is the key equipment to perform the proposed technique, and the demand of AWG on bandwidth and memory is comparative to fast BOTDA based on frequency-agile techniques [17,18]. So it is easy to achieve the proposed fast long-range technique by a commercial AWG.

**Funding.** National Key Scientific Instrument and Equipment Development Project of China (2017YFF0108700); National Natural Science Foundation of China (NSFC) (61575052); Natural Science Foundation of Heilongjiang Province (QC2015087).

## REFERENCES


1. A. Denisov, M. A. Soto, and L. Thévenaz, Light Sci. Appl. **5**, e16074 (2016).
2. Y. Mizuno, N. Hayashi, and H. Fukuda, Light Sci. Appl. **5**, e16184 (2016).
3. M. A. Soto, J. A. Ramirez, and L. Thévenaz, Nat. Commun. **7**, 10870 (2016).
4. S. M. Foaleng, F. Rodríguez-Barrios, and S. Martin-Lopez, Opt. Lett. **36**, 97 (2011).
5. M. Alem, M. A. Soto, and L. Thévenaz, Opt. Express **23**, 29514 (2015).
6. G. L. Keaton, M. J. Leonardo, and M. W. Byer, Opt. Express **22**, 13351 (2014).
7. L. Thévenaz, S. F. Mafang, and J. Lin, Opt. Express **21**, 14017 (2013).
8. Y. Dong, L. Chen, and X. Bao, J. Lightwave Technol. **30**, 1161 (2012).
9. M. A. Soto, G. Bolognini, and F. D. Pasquale, Opt. Lett. **36**, 232 (2011).
10. X. Angulo-Vinuesa, S. Martin-Lopez, and P. Corredera, Opt. Express **20**, 12147 (2012).
11. J. Urricelqui, M. Sagues, and A. Loayssa, Opt. Express **23**, 30448 (2015).
12. M. A. Soto, G. Bolognini, and F. D. Pasquale, Opt. Lett. **35**, 259 (2010).
13. H. Wu, L. Wang, and Z. Zhao, Opt. Express **26**, 5126 (2018).
14. Y. Dong, L. Chen, and X. Bao, Opt. Lett. **36**, 277 (2011).
15. J. J. Mompó, J. Urricelqui, and A. Loayssa, Opt. Express **24**, 12672 (2016).
16. X. Jia, H. Chang, and K. Lin, Opt. Express **25**, 6997 (2017).
17. D. Zhou, Y. Dong, and B. Wang, Light Sci. Appl. **7**, 32 (2018).
18. D. Ba, D. Zhou, and B. Wang, IEEE Photon. J. **9**, 7102908 (2017).